N#-Methylation of arginine: Implications for cell-penetrating peptides

Massachusetts Institute of Technology

RESEARCH ARTICLE

Nα-Methylation of arginine: Implications for cell-penetrating peptides

Lindsey O. Calabretta [ORCID] | **Jinyi Yang** [ORCID] | **Ronald T. Raines** [ORCID]

Department of Chemistry, Massachusetts Institute of Technology, Cambridge, Massachusetts, USA

Correspondence
Ronald T. Raines, Department of Chemistry, Massachusetts Institute of Technology, Cambridge, MA 02139, USA.
Email: rtraines@mit.edu

The field of cell-penetrating peptides is dominated by the use of oligomers of arginine residues. Octanol–water partitioning in the presence of an anionic lipid is a validated proxy for cell-penetrative efficacy. Here, we add one, two, or three *N*-methyl groups to Ac-Arg-NH$_2$ and examine the effects on octanol–water partitioning. In the absence of an anionic lipid, none of these arginine derivatives can be detected in the octanol layer. In the presence of sodium dodecanoate, however, increasing *N*-methylation correlates with increasing partitioning into octanol, which is predictive of higher cell-penetrative ability. We then evaluated fully *N*α-methylated oligoarginine peptides and observed an increase in their cellular penetration compared with canonical oligoarginine peptides in some contexts. These findings indicate that a simple modification, *N*α-methylation, can enhance the performance of cell-penetrating peptides.

KEYWORDS
guanidino group, octanol–water partitioning, peptoid, topological polar surface area

1 | INTRODUCTION

The *N*α-methylation of the main chain in a peptide converts a secondary amido group into a tertiary amido group. Doig and others have used *N*α-methylated peptides as antagonists of β-sheet formation in the context of amyloidogenic peptides.[1–6] Still others have used *N*α-methylation to improve the intestinal uptake, cell permeability, and metabolic stability of peptides and peptide-like molecules.[7–19]

The use of *N*α-methylation as a method to increase cell permeability has taken inspiration from a natural product, cyclosporine A (CsA). CsA is a cyclic peptide that is remarkably cell-permeable due, in part, to the *N*α-methylation of seven main-chain amido groups. This replacement of N–H with N–CH$_3$ eliminates the ability to donate a hydrogen bond to solvent water molecules and thereby reduces the

energetic cost of desolvation that is necessary for crossing a lipid bilayer.[20] Many other natural cyclic peptides are likewise *N*-methylated on their main chain.[21–23]

A powerful method to increase the cellular uptake of cargo has been to append a cell-penetrating peptide (CPP).[24–32] Inspired by the trans-acting activator of transcription (TAT) peptide derived from the human immunodeficiency virus-1 (HIV-1), CPPs are rich in arginine residues. The binding of guanidinium groups to cell-surface oxoanions can facilitate the transport of the peptide and pendant cargo into cells through endocytosis or direct translocation.[24–32]

Wender and coworkers have explored CPPs based on peptoids, which are *N*-alkylated glycine oligomers. They found that peptoid-based CPPs are more cell-permeable than peptide-based CPPs.[33] Similarly, Tan and coworkers screened a large library of peptides and peptoids and found that peptoids are generally more cell-penetrating than peptides.[34] Although peptoids exhibit greater cell permeability than do peptides, commercial monomers for the synthesis of peptoids

The article is dedicated to the memory of Ulf Diederichsen.

Lindsey O. Calabretta and Jinyi Yang contributed equally.

are more costly than those for the synthesis of cognate N^α-methyl peptides.

To our knowledge, these two stratagems for cellular penetration—CPPs and N^α-methylation—have yet to be used in combination. Here, we examine whether an N^α-methylated arginine residue has the physicochemical attributes desirable for cellular penetration, both alone and in the context of an oligomer.

2 | MATERIALS AND METHODS

2.1 | General experimental

2.1.1 | Materials

Commercial compounds were from Sigma-Aldrich (St. Louis, MO), Chem-Impex International (Wood Dale, IL), Ambeed (Arlington Heights, IL), and CEM Corporation (Matthews, NC) and were used without further purification.

2.1.2 | Conditions

All procedures were performed in air at ambient temperature ($\sim 22^\circ$C) and pressure (1.0 atm) unless specified otherwise.

2.1.3 | Solvent removal

The phrase "concentrated under reduced pressure" refers to the removal of solvents and other volatile materials using a rotary evaporator while maintaining a water-bath temperature at 40°C. Residual solvent was removed from samples at high vacuum (<0.1 Torr), which refers to the vacuum achieved by a mechanical belt-drive oil pump or through lyophilization (freeze-drying) using a Labconco FreeZone freeze dryer.

2.1.4 | Chromatography

Chemical reactions were monitored by thin-layer chromatography (TLC) using EMD 250-μm silica gel 60-F_{254} plates and visualization with ultraviolet (UV) illumination or $KMnO_4$ staining, or by liquid chromatography–mass spectrometry (LC–MS) with an ESI Agilent 6125B mass spectrometer. Flash chromatography was performed with a Biotage Isolera automated purification system using prepacked and re-packed SNAP KP silica gel columns and SNAP KP C18 columns.

2.1.5 | Instrumentation

^{1}H-nuclear magnetic resonance (NMR) and ^{13}C-NMR spectra for compound characterization were obtained with Bruker spectrometers. UV

absorbance was measured with a DS-11 spectrophotometer from DeNovix (Wilmington, DE).

High-resolution mass spectrometry (HRMS) data were obtained with an Agilent 6545 quadrupole time-of-flight (Q-TOF) mass spectrometer. Matrix-assisted laser desorption/ionization (MALDI)–TOF analyses were carried out on a microflex® LRF mass spectrometer from Bruker (Billerica, MA) using a saturated solution of α-cyano-4-hydroxycinnamic acid in CH_3CN/water containing TFA (0.1% v/v).

Peptides were synthesized with a Liberty Blue™ automated microwave-assisted peptide synthesizer from CEM (Matthews, NC).

Preparative high-performance liquid chromatography (HPLC) was performed with an Agilent 1260 Infinity II instrument equipped with an XSelect Peptide CSH C18 OBD preparative column from Waters (Milford, MA). Analytical HPLC was performed with an Agilent 1260 Infinity II equipped with an XSelect CSH C18 column from Waters (Milford, MA).

2.2 | Chemical synthesis

The unmethylated compound, Ac-Arg-NH_2 (**1**), was obtained from a commercial vendor as an acetate salt or was synthesized from H-Arg-$NH_2 \cdot 2$HCl using the *N*-acetylation conditions described below. The mono- and di-*N*-methylated compounds, Ac-Arg-NHMe (**2**) and Ac-Arg-NMe_2 (**3**), were synthesized by the sequential use of thionyl chloride plus an amine and then acetic anhydride as in the initial and final steps in the route to compound **4** (Scheme [1]). Later, we acquired Fmoc-*N*-Me-Arg (Pbf)-OH and used this shorter route to produce compound **4**. Compounds **1**–**4** were converted to the desired chloride salt by using a guanidine resin charged with HCl, as described previously.[35]

2.2.1 | H-Arg(Pbf)-NMe_2 (**5**)

Fmoc-Arg(Pbf)-OH (2 g, 3 mmol) was placed in a dry flask. Thionyl chloride (5 mL) was added, and the yellow solution was stirred under N_2(g) for 45 min. The acyl chloride intermediate was concentrated under reduced pressure, dissolved in 5 mL of dry THF, and concentrated again to remove any remaining thionyl chloride. The resulting tan foam was dissolved in 5 mL of dry THF, and the solution was cooled under N_2(g) in an ice bath. A 2-M solution of dimethylamine in THF (25 mL, 50 mmol) was added dropwise. After that addition, the resulting solution was stirred overnight. The solution was then vacuum-filtered to remove the dimethylamine salts and concentrated under reduced pressure. The resulting oil was then redissolved in morpholine, and the resulting solution was stirred for 1 h and again concentrated under reduced pressure. The crude oil was purified by chromatography on silica gel with a MeOH/DCM gradient, eluting at 20% v/v MeOH to produce compound **5** as a white foam (1.23 g, 57% yield). ^{1}H-NMR (500 MHz, CDCl$_3$, δ): 6.60 (br, 1H), 6.45 (br, 2H), 3.76 (dd, $J = 8.4$, 3.8 Hz, 1H), 3.20 (br, 2H), 3.00 (s, 3H), 2.95 (s, 2H), 2.93 (s, 3H), 2.57 (s, 3H), 2.50 (s, 3H), 2.35 (br, 2H), 2.08 (s, 3H), 1.73–1.55

SCHEME 1 Synthetic route to Ac-(*N*-Me)Arg-NMe$_2$ (**4**)
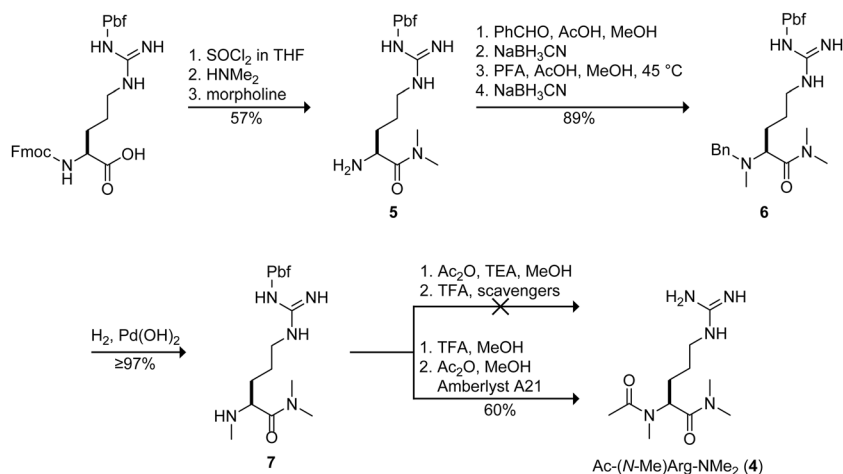
(m, 3H), 1.46 (s, 6H), 1.46 (m, 1H). ^{13}C-NMR (500 MHz, CDCl$_3$, δ): 174.74, 158.64, 156.40, 138.24, 133.13, 132.19, 124.56, 117.42, 86.35, 50.69, 43.25, 40.81, 36.89, 35.90, 28.60, 28.59, 25.55, 19.27, 17.92, 12.48. HRMS *m/z* calcd for C$_{21}$H$_{35}$N$_5$O$_4$S [M+H]$^+$, 454.2488; found, 454.2483.

2.2.2 | *N*-Bn-*N*-Me-Arg(Pbf)-NMe$_2$ (**6**)

H-Arg(Pbf)-NMe$_2$ (**5**) (200 mg, 0.44 mmol) was dissolved in methanol (5 mL). Benzaldehyde (48 μL, 0.48 mmol) and acetic acid (25 μL, 0.44 mmol) were added, and the resulting solution was stirred for 2 h. Sodium cyanoborohydride (30 mg, 0.48 mmol) was added, and the resulting solution was stirred overnight. Paraformaldehyde (PFA) (14.4 mg, 0.48 mmol) and acetic acid (25 μL, 0.44 mmol) were added, and the resulting solution was stirred at 40°C for 1 h. Sodium cyanoborohydride (30 mg, 0.48 mmol) was dissolved in 1 mL of acetonitrile, and the resulting solution was added to the reaction mixture over 10 h via a syringe pump. After another 8 h, the solution was concentrated under reduced pressure. To remove excess cyanoborohydride, the crude product was dissolved in 5 mL of methanol and 1 mL of acetic acid, and the resulting solution was concentrated under reduced pressure, and then the process was repeated. The crude product was dissolved in water and extracted three times with dichloromethane. The organic layers were combined, dried over Na$_2$SO$_4$(s), and filtered. The crude product was purified by chromatography on silica gel with a MeOH/DCM gradient, eluting at 8% v/v MeOH to produce compound **6** as a white foam (219 g, 89% yield). ^{1}H-NMR (500 MHz, CDCl$_3$, δ): 7.33–7.27 (m, 2H), 7.27–7.22 (m, 3H), 6.17 (br, 1H), 6.08 (br, 2H), 3.62 (d, *J* = 13.3 Hz, 1H), 3.53 (d, *J* = 13.3 Hz, 1H), 3.46 (dd, *J* = 10.2, 3.7 Hz, 1H), 3.19 (br, 2H), 3.05 (s, 3H), 2.94 (s, 2H), 2.94 (s, 3H), 2.60 (s, 3H), 2.54 (s, 3H), 2.19 (s, 3H), 2.09 (s, 3H), 1.95–1.81 (m, 1H), 1.75–1.66 (m, 1H), 1.59–1.48 (m, 1H), 1.45 (s, 6H), 1.39–1.27 (m, 1H). ^{13}C-NMR (500 MHz, CDCl$_3$, δ): 172.00, 158.60, 156.11, 138.74, 138.39, 133.22, 132.33, 128.82, 128.33, 127.22, 124.48, 117.37, 86.28, 63.35, 58.01, 43.26, 41.20, 37.85, 37.33, 36.04,

28.60, 28.59, 26.31, 19.27, 17.92, 12.47. HRMS *m/z* calcd for C$_{29}$H$_{43}$N$_5$O$_4$S [M+H]$^+$, 558.3114; found, 558.3115.

2.2.3 | Me-Arg(Pbf)-NMe$_2$ (**7**)

Method 1

N-Bn-*N*-Me-Arg(Pbf)-NMe$_2$ (**6**) (100 mg, 0.18 mmol) was dissolved in methanol (2 mL). The resulting solution was sparged with N$_2$(g) for 10 min. Palladium hydroxide (15 mg, 15% wt) was added, and the resulting solution was sparged with H$_2$(g) for 15 min. Then, the solution was stirred under a balloon of H$_2$(g) overnight. The reaction mixture was filtered through celite and concentrated under reduced pressure to produce compound **7** as a white foam (76 mg, quantitative yield), which was used directly.

Method 2

Fmoc-*N*-Me-Arg(Pbf)-OH (613 mg, 0.92 mmol) was placed in a dry flask. Thionyl chloride (5 mL) was added, and the resulting yellow solution was stirred under N$_2$(g) for 1 h. The acyl chloride intermediate was concentrated under reduced pressure, dissolved in 5 mL of dry THF, and concentrated again to remove any remaining thionyl chloride. The resulting tan foam was dissolved in 2 mL of dry THF, and the solution was cooled under N$_2$(g) in an ice bath. A 2-M solution of dimethylamine in THF (5 mL, 10 mmol) was added dropwise, and the solution was stirred for 1 h. The solution was then vacuum-filtered to remove the dimethylammonium salts and concentrated under reduced pressure. The resulting foam was then redissolved in a 2 M solution of methylamine in MeOH (5 mL), and the resulting solution was stirred for 1 h and again concentrated under reduced pressure. The crude oil was purified by chromatography on silica gel with a MeOH/DCM gradient, eluting at 15% v/v MeOH to produce compound **7** as a white foam (454 mg, 97% yield.)

^{1}H-NMR (500 MHz, CDCl$_3$, δ): 6.78 (br, 1H), 6.55 (br, 3H), 3.84 (m, 1H), 3.46 (s, 3H), 3.22 (t, *J* = 6.7 Hz, 2H), 3.07 (s, 3H), 2.99 (s, 3H), 2.95 (s, 3H), 2.57 (s, 3H), 2.50 (s, 3H), 2.08 (s, 3H), 1.87–1.76 (m, 1H), 1.76–1.55 (m, 3H), 1.46 (s, 6H). ^{13}C-NMR (500 MHz, CDCl$_3$, δ):

177.41, 158.66, 156.58, 138.25, 133.00, 132.19, 124.58, 117.46, 86.37, 59.04, 43.25, 40.50, 37.09, 35.96, 33.93, 28.78, 28.59, 24.94, 19.27, 17.94, 12.47. HRMS m/z calcd for $C_{22}H_{37}N_5O_4S$ $[M + H]^+$, 468.2645; found, 468.2638.

2.2.4 | *N*-Acetyl-*N*-Me-Arg-NMe$_2$·HCl (**4**·HCl)

Me-Arg(Pbf)-NMe$_2$ (**7**) (532 mg, 1.14 mmol) was placed in a flask, followed by methanol (100 μL) and trifluoroacetic acid (3 mL). After 1.5 h, the trifluoroacetic acid was evaporated under a stream of $N_2(g)$. The deprotected product was then dissolved in water and extracted with DCM two times. The greenish organic fractions were discarded, and the aqueous fractions were combined and lyophilized. The crude intermediate was dissolved in methanol (12 mL), and Amberlyst A21 was added until the pH was above 7 (1.5 g). Acetic anhydride (323 μL, 3.4 mmol) was added, and the resulting solution was stirred for 3 h. The solution was filtered to remove the resin and concentrated under reduced pressure. The product was purified by reversed-phase chromatography in H_2O. The product was then flushed through an *N*-dimethylaminopropyl-*N*′-ethylguanidine resin pipette column charged with HCl and lyophilized to produce compound **2**·HCl as a white powder (200 mg, 60% yield). ^1H-NMR (400 MHz, D$_2$O, δ): 5.33 (dd, $J = 8.8, 6.0$ Hz, 1H), 3.22 (t, $J = 6.9$, 1H), 3.21 (t, $J = 6.9$, 1H), 3.00 (s, 3H), 2.96 (s, 3H), 2.92 (s, 3H), 2.18 (s, 3H), 1.94 (s, 3H, CH$_3$COOH), 1.77 (m, 2H), 1.53 (p, $J = 7.3$ Hz, 2H). ^{13}C-NMR (400 MHz, D$_2$O, δ): 180.94, 174.26, 171.39, 156.70, 53.35, 40.66, 36.71, 35.88, 31.18, 25.20, 24.20, 22.95, 20.88. HRMS m/z calcd for $C_{11}H_{23}N_5O_2$ $[M+H]^+$, 258.1930; found, 258.1922.

2.2.5 | H-Arg(Pbf)-NHMe (**8**)

Fmoc-Arg(Pbf)-OH (2 g, 3 mmol) was placed in a dry flask. Thionyl chloride (5 mL) was added, and the yellow solution was stirred under $N_2(g)$ for 1 h. The acyl chloride intermediate was concentrated under reduced pressure, dissolved in 5 mL of dry THF, and concentrated again to remove any remaining thionyl chloride. The resulting tan foam was dissolved in 5 mL of dry THF, and the solution was cooled under $N_2(g)$ in an ice bath. A 2 M solution of methylamine in THF (15 mL, 30 mmol) was added dropwise, and the solution was stirred for 1 h. The solution was then vacuum-filtered to remove the dimethylamine salts and concentrated under reduced pressure. The resulting foam was then redissolved in a 2-M solution of methylamine in MeOH (10 mL), and the resulting solution was stirred for 1 h and again concentrated under reduced pressure. The crude oil was purified by chromatography on silica gel with a MeOH/DCM gradient, eluting at 15% v/v MeOH to produce compound **8** as a white foam (1.05 g, 80% yield). ^1H-NMR (500 MHz, CDCl$_3$, δ): 7.61 (d (br), $J = 6.4$ Hz, 1H), 6.51 (t (br), $J = 5.6$ Hz, 1H), 6.42 (s (br), 2H), 3.53 (t, $J = 6.5$ Hz, 1H), 3.22 (t, $J = 6.4$ Hz, 2H), 2.95 (s, 2H), 2.56 (s, 3H), 2.49 (s, 3H), 2.17 (s, 3H), 2.08 (s, 3H), 1.88–1.73 (m, 1H), 1.69–1.54 (m, 3H), 1.46 (s, 6H). ^{13}C-NMR (500 MHz, CDCl$_3$, δ): 175.14, 158.79,

156.50, 138.27, 132.73, 132.20, 124.69, 117.58, 86.45, 54.10, 43.24, 40.47, 31.65, 30.94, 28.60, 25.40, 25.34, 19.28, 17.94, 12.48. HRMS m/z calcd for $C_{20}H_{34}N_5O_4S$ $[M+H]^+$, 440.2332; found, 440.2325.

2.2.6 | *N*-Acetyl-Arg-NHMe·HCl (**2**·HCl)

H-Arg(Pbf)-NHMe (**8**) (440 mg, 1 mmol) was placed in a flask, followed by methanol (100 μL) and trifluoroacetic acid (3 mL). After 1 h, the trifluoroacetic acid was evaporated under a stream of $N_2(g)$. The deprotected product was then dissolved in water and extracted with DCM two times. The greenish organic fractions were discarded, and the aqueous fractions were combined and evaporated under reduced pressure. The resulting oil was dissolved in MeOH (10 mL), and Amberlyst A21 free base (1.5 g) and acetic anhydride (284 μL, 3 mmol) were added to the flask. The resulting solution was stirred for 3 h. The solution was filtered to remove the resin and concentrated under reduced pressure. The product was purified by reversed-phase chromatography in H_2O. The product was then flushed through a *N*-dimethylaminopropyl-*N*′-ethylguanidine resin pipette column charged with HCl and lyophilized to produce compound **2**·HCl as a hard colorless foam (160 mg, 60% yield). ^1H-NMR (600 MHz, DMSO-d_6, δ): 8.10 (d, $J = 8.1$ Hz, 1H), 8.04 (s, 1H), 7.97 (d, $J = 5.0$ Hz, 1H), 7.28 (br, 4H), 4.18 (q, $J = 7.7, 7.1$ Hz, 1H), 3.08 (t, $J = 6.3$ Hz, 2H), 2.57 (d, $J = 4.4$ Hz, 3H), 1.86 (s, 3H), 1.71–1.61 (m, 1H), 1.56–1.34 (m, 3H). ^{13}C-NMR (600 MHz, DMSO-d_6, δ): 172.39, 169.79, 157.46, 52.54, 40.64, 29.56, 25.97, 25.62, 23.03. HRMS m/z calcd for $C_9H_{20}N_5O_2$ $[M+H]^+$, 230.1617; found, 230.1608.

2.2.7 | *N*-Acetyl-Arg-NMe$_2$·HCl (**3**·HCl)

H-Arg(Pbf)-NMe$_2$ (**5**) (453 mg, 1 mmol) was placed in a flask, followed by methanol (100 μL) and trifluoroacetic acid (3 mL). After 1 h, the trifluoroacetic acid was evaporated under a stream of $N_2(g)$. The deprotected product was then dissolved in water and extracted with DCM two times. The greenish organic fractions were discarded, and the aqueous fractions were combined and evaporated under reduced pressure. The resulting oil was dissolved in MeOH (10 mL), and Amberlyst A21 free base (1.5 g) and acetic anhydride (284 μL, 3 mmol) were added to the flask. The resulting solution was stirred for 3 h. The solution was filtered to remove the resin and concentrated under reduced pressure. The product was purified by reversed-phase chromatography in H_2O. The product was then flushed through an *N*-dimethylaminopropyl-*N*′-ethylguanidine resin pipette column charged with HCl and lyophilized to produce compound **3**·HCl as a white powder (132 mg, 47% yield). ^1H-NMR (600 MHz, DMSO-d_6 δ): 8.14 (d, $J = 8.3$ Hz, 1H), 7.75 (t, $J = 5.8$ Hz, 1H), 7.39 (br, 2H), 6.95 (br, 2H), 4.69 (q, $J = 6.7$ Hz, 1H), 3.15–3.05 (m, 2H), 3.02 (s, 3H), 2.83 (s, 3H), 1.84 (s, 3H), 1.70–1.53 (m, 1H), 1.55–1.37 (m, 3H). ^{13}C-NMR (600 MHz, DMSO-d_6 δ): 171.56, 169.46, 157.35, 48.26, 40.87, 37.07, 35.65, 29.16, 25.35, 22.77. HRMS m/z calcd for $C_{10}H_{21}N_5O_2$ $[M+H]^+$, 244.1774; found, 244.1765.

2.3 | Octanol–water partitioning experiments

Procedures for the octanol–water partitioning experiment were similar to those reported previously[35] and are described in detail below.

Ac-Arg-NH$_2$·HCl (**1**·HCl) (27.7 mg, 0.11 mmol) was dissolved in D$_2$O (5.5 mL) to make a 0.02 M stock solution. Six Eppendorf tubes were prepared, three of which contained sodium dodecanoate (8.9 mg, 0.04 mmol, 2.5 equiv of **1**·HCl). An 800-μL aliquot of the arginine stock solution was pipetted into each of the six tubes. An 800-μL aliquot of octanol was then partitioned into each tube. The tubes were vortexed for 30 s, then subjected to centrifugation for 15 min. Once the layers had separated, a 200-μL aliquot was removed carefully from the aqueous layers with a pipette and added to a new tube. A 200-μL aliquot of the unadulterated stock was also placed in a new tube. A solution of 0.2 M pyridine in D$_2$O (20 μL) was added to each tube, the tubes were shaken, and the solutions were transferred to 3-mm NMR tubes for analysis. This procedure was repeated with **2**·HCl, **3**·HCl, and **4**·HCl.

^{1}H-NMR spectra of the aliquots were collected with a 20-s relaxation delay (D1) to ensure quantitative integrations between the pyridine and amino acid residue. Spectral integrations were referenced to the signal of the *para*-hydrogen of pyridine, and the integration of the signal from the H$^\delta$ protons of the amino acid residue was measured. The relative integrations pre- and post-wash were compared with each other. For all amino acid residues, the spectra following the octanol washes showed a slightly higher integration. This increase was likely the result of a small amount of octanol remaining in the water layer. Because the amount of additional integration in the post-octanol and octanol + lipid washes is likely to be the same, we evaluated the extent of partitioning by determining the difference between the octanol and octanol + lipid washes and averaging the values from the three replicates.

2.4 | Peptide synthesis

Peptides were synthesized on Rink Amide ProTide® resin (0.59 mmol/g) at a 50-μmol scale. Canonical polyarginine peptides, fluorescein-Ahx-(Arg)$_5$-NH$_2$ (**R$_5$**), and fluorescein-Ahx-(Arg)$_8$-NH$_2$ (**R$_8$**) were synthesized by automated solid-phase peptide synthesis (SPPS). The general coupling method was employed as follows: 2-min coupling (90°C), 1-min deprotection (90°C), and 1-min associated washes and liquid handling. Fmoc removal was achieved in 4-methyl piperidine (20% v/v in DMF), and Fmoc-protected amino acid monomer (5 equiv), activated with DIC and Oxyma, was coupled to the free amino group on the growing chain. N^α-methylated oligoarginine peptides, fluorescein-Ahx-(N^α-Me-Arg)$_5$-NH$_2$ (Me-**R$_5$**) and fluorescein-Ahx-(N^α-Me-Arg)$_8$-NH$_2$ (Me-**R$_8$**), were synthesized by manual SPPS with 2.5 equiv of monomer at 37°C. Peptides were cleaved from the resin and globally deprotected in 2.0 mL of reagent K, which was 85:5:5:2.5:2.5 TFA/phenol/thioanisole/2,2′-(ethylenedioxy)di-ethanethiol/water, precipitated from pre-cooled diethyl ether, and isolated by centrifugation. Dried crude peptides were dissolved in TFA (0.1% v/v), filtered, and purified by preparative HPLC using a linear gradient of CH$_3$CN in water containing TFA (0.1% v/v). All peptides were >90% pure according to analytical HPLC and MALDI–TOF mass spectrometry. Peptide concentrations were standardized using the fluorescence absorbance of fluorescein at 490 nm.

2.5 | Mammalian cell culture

HeLa cells were from the American Tissue Culture Collection and cultured according to recommended protocols. Cells were grown in Dulbecco's modified Eagle's medium (DMEM) supplemented with fetal bovine serum (10% v/v), penicillin (100 units/mL), and streptomycin (100 μg/mL). Cells were grown in T75 sterile culture flasks in a cell culture incubator at 37°C under CO$_2$ (5% v/v). Cells were counted to determine seeding density using a hemacytometer.

2.6 | Flow cytometry

HeLa cells were seeded at a density of 50 000 cell/well in a sterile 8-well dish (LabTek) 24 h prior to treatment. Cells were incubated with 1 μM of a canonical oligoarginine peptide or N^α-methylated oligoarginine peptide in DMEM medium supplemented with fetal bovine serum (10% v/v), penicillin (100 units/mL), and streptomycin (100 μg/mL) for 1 h at 37°C. Cells were rinsed twice with DPBS and released from the plate by treatment with 200 μL of 0.25% v/v trypsin–EDTA mix. Trypsin was quenched by adding 400 μL of medium, and samples were strained through flow cytometry tubes. Cells were subjected to centrifugation at 200 g for 5 min at 4°C. Pellets were resuspended and washed three times in DPBS supplemented with bovine serum albumin (0.1% v/v). SYTOX AADvanced™ ready flow™ reagent was added to each sample according to the manufacturer's protocol, and cells were kept on ice until the time of analysis. The fluorescence intensity of at least 10 000 events was measured by flow cytometry with an Attune NxT flow cytometer (488-nm laser with a detector bandpass of 530/30 nm for fluorescein and 561-nm laser with a detector bandpass of 620/15 nm for SYTOX AADvanced™, Thermo-Fisher Scientific). Fluorescence compensation was determined experimentally and applied automatically by the instrument. Data analysis was done with FlowJo software. Values are the geometric means of the green fluorescence of live, single cells from excitation with a 488-nm laser.

3 | RESULTS AND DISCUSSION

For our physicochemical analyses, we used four arginine derivatives: Ac-Arg-NH$_2$ (**1**) and its *N*-methylated analogs: Ac-Arg-NHMe (**2**), Ac-Arg-NMe$_2$ (**3**), and Ac-(*N*-Me)Arg-NMe$_2$ (**4**) (Scheme 2). As a proxy for cellular penetration, we used the method pioneered by Rothbard and Wender, who established that partitioning from water into octanol in the presence of an anionic lipid correlates with cell-penetration ability.
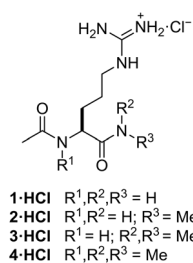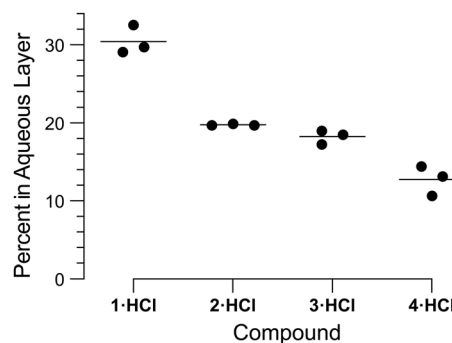
SCHEME 2   Structures of Ac-Arg-NH$_2$·HCl (**1**·HCl), Ac-Arg-NHMe·HCl (**2**·HCl), Ac-Arg-NMe$_2$·HCl (**3**·HCl), and Ac-(*N*-Me)Arg-NMe$_2$·HCl (**4**·HCl)

FIGURE 1   Graph showing the extent of octanol–water partitioning of compounds **1**–**4**·HCl in the presence of sodium dodecanoate (2.5 equiv).[35,37] Values were determined by [1]H-nuclear magnetic resonance (NMR) spectroscopy. See Figures S1–S4 for representative spectra.

For example, Arg$_9$ partitions into octanol in the presence of dodecanoate; whereas, Orn$_9$ (which is a nonamer of L-ornithine) does not; likewise, they also observed that Arg$_9$ is taken up into cells, and Orn$_9$ is not.[36,37]

To access tri-*N*-methylated analog Ac-(*N*-Me)Arg-NMe$_2$ (**4**), we converted commercial Fmoc-Arg(Pbf)-OH into a dimethyl amide (**5**) (Scheme 1). Our initial attempts to do so used traditional coupling methods, such as HATU in DMF. These methods resulted in low yields and difficulty in separating the polar product from the coupling reagent. Instead, we converted the carboxyl group of Fmoc-Arg(Pbf)-OH into an acyl chloride with SOCl$_2$ and produced dimethyl amide **5** with the addition of dimethylamine.[38] The dimethylamine was also partially successful at inciting a β-elimination to remove the Fmoc group, and morpholine was used to entice the elimination of remaining Fmoc groups. Next, we sought to append a single methyl group to the N-terminal amino group. With the use of an approach inspired by White and Konopelski,[39] we installed a benzyl and a methyl group on the amino group through iterative reductive amination reactions with benzaldehyde and PFA to produce compound **6**. Subsequently, we removed the benzyl group by hydrogenolysis to produce compound **7**.

Initially, we attempted to install an acetyl group on compound **7** by using acetic anhydride, followed by the removal of the Pbf group[40] with TFA in the presence of scavengers, such as ethanethiol and phenylsilane. Surprisingly, these conditions resulted in the hydrolysis of the dimethyl amide along with the removal of the Pbf group. In hindsight, we realized that amides in close proximity to carboxyl groups could suffer rapid hydrolysis.[41,42] We hypothesize that, in acidic conditions, the acetyl oxygen attacks the protonated C-terminal amide to form a five-membered ring, which leads to the hydrolysis of the C-terminal amide. We obtained conformational data for compound **4** using selective 1D NOESY (vide infra) and found that its carbonyl group is preorganized for this intramolecular attack (Figure S6). To avoid this degradative route, we first removed the Pbf group by treating with TFA and then appended the acetyl group by using acetic anhydride and the tertiary amino resin Amberlyst A21 to produce the desired compound, Ac-(*N*-Me)Arg-NMe$_2$ (**4**).

With compounds **1**–**4**·HCl in hand, we compared their ability to partition from water into octanol in the presence and absence of an anionic lipid, sodium dodecanoate. Previously, we used this anion-mediated octanol–water partitioning to compare the partitioning of L-

canavanine (which is δ-oxa-arginine) to that of arginine.[35] Here, we used this method to compare the partitioning of compounds **1**–**4**·HCl (Figures S1–S4). To do so, we prepared solutions of each compound in D$_2$O and added octanol. We carefully extracted an aliquot of the D$_2$O layer and spiked it with a known quantity of a reference compound (pyridine) as an internal standard. Then, we used ^{1}H-NMR spectroscopy to determine the concentration of compounds **1**–**4** that remained in the water layer after the wash with octanol. We found that all of the compounds remained entirely in the water layer after washing with octanol. Next, we exposed the aqueous solutions of **1**–**4**·HCl to octanol containing sodium dodecanoate. We found that dodecanoate transports all of the compounds into the octanol layer but to varying extents (Figure 1).

We observed a general trend: Increasing the extent of N^α-methylation of Ac-Arg-NH$_2$ decreases its concentration in the water layer after partitioning with octanol plus dodecanoate. The largest differential occurred between compounds with zero methyl groups (**1**) and one methyl group (**2**), with smaller differences between one methyl group (**2**) and two methyl groups (**3**) and between two methyl groups (**3**) and three methyl groups (**4**). Importantly, we did observe a substantial increase in the partitioning into octanol of **4** compared with **2**. These two compounds most accurately mimic the environment in the middle of an unmodified peptide (**2**) and N^α-methylated peptide (**4**).

To provide insight into the origin of anion-mediated partitioning upon N^α-methylation, we calculated the cLog*P* and topological polar surface area (TPSA) values of all compounds (Table 1). The cLog*P* values of compounds **1**–**4**·H$^+$ show no correlation with the partitioning results. In contrast, the TPSA of each compound does correlate with the partitioning results. With decreasing TPSA, the partitioning of the compound into octanol increases. Moreover, the difference in TPSA between compounds **2** and **3** and between compounds **3** and **4** is 9 Å^2. The difference in TPSA between compounds **1** and **2** is greater at 14 Å^2, analogous to the greater difference in their octanol–water partitioning in the presence of sodium dodecanoate (Figure 1).

TABLE 1 Calculated and experimental parameters of arginine derivatives

Compound	cLogP[a]	TPSA (Å²)[a]	Percent in aqueous layer[b]
Ac-Arg-NH$_2$·H$^+$ (**1**·H$^+$)	−4.63	135.8	30.4 ± 1.5 28.0 ± 0.7[c]
Ac-Arg-NHMe·H$^+$ (**2**·H$^+$)	−4.72	121.8	19.8 ± 0.1
Ac-Arg-NMe$_2$·H$^+$ (**3**·H$^+$)	−4.81	113.0	18.3 ± 0.7
Ac-(*N*-Me)Arg-NMe$_2$·H$^+$ (**4**·H$^+$)	−4.70	104.3	12.7 ± 1.6
Ac-Cav-NH$_2$·H$^+$	−4.90	147.4	85.4 ± 0.6[c]

[a]Values were calculated with software from Molinspiration Cheminformatics (Slovenský Grob, Slovak Republic).

[b]Values are the mean ± SD for octanol–water partitioning in the presence of sodium dodecanate (2.5 equiv), as depicted in Figure 1.

[c]Values are from Calabretta et al.[35]

Previously, we observed that *N*-acetylated canavanine amide (Ac-Cav-NH$_2$) partitions into octanol to a lesser extent than does compound **1** in the presence of dodecanoate.[37] Whereas the TPSAs of compounds **2**·H$^+$, **3**·H$^+$, and **4**·H$^+$ are 14.0, 22.8, and 31.5 Å², respectively, less than that of **1**·H$^+$, the TPSA of Ac-Cav-NH$_2$·H$^+$ is 11.6 Å² greater than that of **1**·H$^+$. The octanol:water partitioning of Ac-Cav-NH$_2$ in the presence of dodecanoate is likewise larger than that of compounds **1**–**4** (Table 1).[37] Thus, TPSA provides a reliable qualitative though not necessarily quantitative prediction of anion-mediated octanol–water partitioning. Similarly, TPSA values correlate inversely with the permeability of small-molecule drugs.[43,44]

We extended this analysis by calculating the TPSA values of a well-known CPP, **R$_8$**, and its *N*$^{\alpha}$-methylated congener, Me-**R$_8$**. We found that Me-**R$_8$** has a significantly lower TPSA value than does **R$_8$** (Table S1). The TPSA calculated for the analogous peptoid, *N*arg$_8$, is also lower than that of **R$_8$** and, remarkably, results in exactly the same value as Me-**R$_8$**. These calculated values correlate with the experimental data of Tan and coworkers, who observed that peptoids had, in general, a lower TPSA and higher cell permeability than do peptides and that peptoids with especially small TPSA values had enhanced cell permeability.[34]

N$^{\alpha}$-Methylation is known to influence the conformation of peptides.[45] We noticed that in D$_2$O solutions, the signal for the δ protons of compounds **1**–**3** was a triplet, whereas the signal for compound **4** was two overlapping doublets of triplets with the doublet $J \approx 20$ Hz being indicative of geminal coupling. The different δ proton environments suggested that the conformation of compound **4** is more constrained than that of the other amino acids. Accordingly, we performed selective 1D NOESY on all protons of compound **4** (Figure S5). We observed through-space correlations that indicate that the rotation of the N–C$^{\alpha}$ and C$^{\alpha}$–C′ bonds is indeed restricted.

Arvidsson and coworkers have reported crystal structures of poly-*N*$^{\alpha}$-methylated peptides and determined that they adopt an all-*trans* extended conformation reminiscent of a β-strand.[46] Polymers of *N*$^{\alpha}$-Me-Ala adopt two main-chain conformations, one of which has a C$_{Me}$–N–C$^{\alpha}$–C$^{\beta}$ torsion angle of about −68°. The NOESY correlations that we observed are consistent with this conformation (Figure S6). The secondary structure of CPPs is known to influence their efficiency and
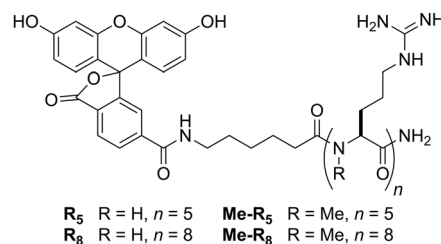
SCHEME 3 Structures of fluorescein-Ahx-(Arg)$_5$-NH$_2$ (**R$_5$**), fluorescein-Ahx-(*N*$^{\alpha}$-Me-Arg)$_5$-NH$_2$ (Me-**R$_5$**), fluorescein-Ahx-(Arg)$_8$-NH$_2$ (**R$_8$**), and fluorescein-Ahx-(*N*$^{\alpha}$-Me-Arg)$_8$-NH$_2$ (Me-**R$_8$**)
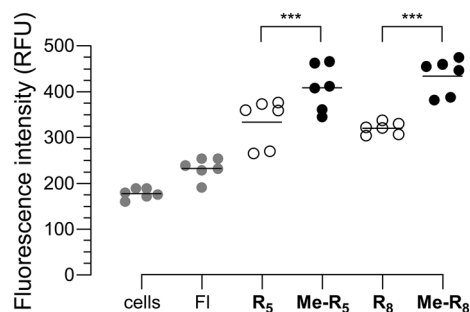
FIGURE 2 Graph showing the uptake of cell-penetrating peptides (CPPs) by live HeLa cells using flow cytometry. Cells were treated with 1 μM of carboxyfluorescein (Fl) or fluorescein-labeled oligoarginine for 1 h at 37°C. Geometric mean values of the green fluorescence from living, single cells were recorded by flow cytometry. *P* values were calculated with a paired two-tailed *t* test; ***$P < 0.001$.

pathway of uptake.[47,48] Thus, the conformational rigidity in *N*$^{\alpha}$-methylated CPPs could influence their cell-penetrative ability.

To explore further the effect of the *N*$^{\alpha}$-methylation of arginines, we compared the cellular uptake efficiency of fully *N*$^{\alpha}$-methylated oligoarginine peptides with canonical oligoarginine peptides of the same length. We used commercially available Fmoc-*N*-Me-Arg (Pbf)-OH to access *N*$^{\alpha}$-methylated polypeptides (Scheme 3; Figures S7–S10). We evaluated Me-**R$_5$** and Me-**R$_8$**, as both **R$_5$** and **R$_8$** have been used as CPPs.[49–51] Cell-penetrating abilities were

evaluated in live HeLa cells. All peptides were labeled with fluorescein as a reporter for readout. The cellular uptake of R_5, Me-R_5, R_8, and Me-R_8 was quantified by using flow cytometry.[16,52] Cells were incubated with peptides at 4 or 37°C for 1 h, washed twice with Ca^{2+}- and Mg^{2+}-deficient PBS, trypsinized, and subjected to analysis with flow cytometry.

Whereas untreated cells and fluorescein-treated cells showed minimal fluorescence, cells treated with CPP displayed an elevated fluorescence signal. At low CPP concentrations, the uptake of both penta- and octaarginines is low, but we observed a 23% increase in fluorescence for cells treated with Me-R_5 compared with R_5, and an increase of 34% for cells treated with Me-R_8 compared with R_8 (Figures 2, S11, and S12). These findings are consistent with the octanol–water partitioning of compounds **1**–**4** (Figure 1).

With increasing concentration of the CPPs, the advantage of *N*-methylation in cellular uptake was retained by pentaarginine (Figure S13). In contrast, octaarginine was internalized to a similar or even greater extent than its *N*-methylated counterpart at high concentration at both 37°C and 4°C (Figures S14 and S15). Apparently, the benefit of N^α-methylation is overridden by additional guanidinium groups under some conditions.

4 | CONCLUSIONS

We have discovered that N^α-methylated arginine monomers partition more into octanol in the presence of an anionic lipid than does a non-methylated monomer. That finding led us to compare fully N^α-methylated oligoarginine peptides with congeners of the same length, and we observed enhanced cell-permeability upon N^α-methylation. In displaying a guanidinium group but not an amido N–H group, an N^α-methylated arginine residue is reminiscent of the γ-guanidinoproline residues of Wennemers and coworkers, which are superior to arginine residues at eliciting cellular penetration.[47] In oligoarginines, the benefits of N^α-methylation are manifested more strongly by shorter CPPs or at low CPP concentrations. Notably, N^α-methylated CPPs are easily accessible by SPPS because of the commercial availability of N^α-methylated amino acids. Finally, CPPs based on N^α-methylated amino acid residues might not only demonstrate enhanced cellular uptake but also benefit from greater metabolic stability and other attributes.[7–19]

ORCID

Lindsey O. Calabretta https://orcid.org/0000-0002-5747-5803
Jinyi Yang https://orcid.org/0000-0002-9694-1838
Ronald T. Raines https://orcid.org/0000-0001-7164-1719

REFERENCES

1. Hughes E, Burke RM, Doig AJ. Inhibition of toxicity in the β-amyloid peptide fragment β-(25–35) using *N*-methylated derivatives: a general strategy to prevent amyloid formation. *J Biol Chem*. 2000;275(33): 25109-25115. doi:10.1074/jbc.M003554200

2. Gordon DJ, Sciaretta KL, Meredith SC. Inhibition of β-amyloid (40) fibrillogenesis and disassembly of β-amyloid(40) fibrils by short β-amyloid cogeners containing *N*-methyl amino acids at alternate residues. *Biochemistry*. 2001;40(28):8237-8245. doi:10.1021/bi002416v

3. Gordon DJ, Tappe R, Meredith SC. Design and characterization of a membrane permeable *N*-methyl amino acid-containing peptide that inhibits Aβ(1–40) fibrillogenesis. *J Pept Res*. 2002;60(1):37-55. doi:10.1034/j.1399-3011.2002.11002.x

4. Cruz M, Tusell JM, Grillo-Bosch D, et al. Inhibition of β-amyloid toxicity by short peptides containing *N*-methyl amino acids. *J Pept Res*. 2004;63(3):324-328. doi:10.1111/j.1399-3011.2004.00156.x

5. Kokkoni N, Stott K, Amijee H, Mason JM, Doig AJ. *N*-methylated peptide inhibitors of β-amyloid aggregation and toxicity. Optimization of the inhibitor structure. *Biochemistry*. 2006;45(32):9906-9918.

6. Pratim Bose P, Chatterjee U, Nerelius C, et al. Poly-*N*-methylated amyloid β-peptide (Aβ) C-terminal fragments reduce Aβ toxicity in vitro and in *Drosophila melanogaster*. *J Med Chem*. 2009;52(24): 8002-8009. doi:10.1021/jm901092h

7. Conradi RA, Hilgers AR, Ho NF, Burton PS. The influence of peptide structure on transport across Caco-2 cells. *Pharm Res*. 1991;8(12): 1453-1460. doi:10.1023/A:1015825912542

8. Simon RJ, Kania RS, Zuckermann RN, et al. Peptoids: a modular approach to drug discovery. *Proc Natl Acad Sci U S A*. 1992;89(20): 9367-9371. doi:10.1073/pnas.89.20.9367

9. Haviv F, Fitzpatrick TD, Swenson RE, et al. Effect of *N*-methyl substitution of the peptide bonds in luteinizing hormone-releasing hormone agonists. *J Med Chem*. 1993;36(3):363-369. doi:10.1021/jm00055a007

10. Chikhale EG, Ng KY, Burton PS, Borchardt RT. Hydrogen bonding potential as a determinant of the *in vitro* and *in situ* blood–brain barrier permeability of peptides. *Pharm Res*. 1994;11:412-419.

11. Rennert R, Wespe C, Beck-Sickinger AG, Neundorf I. Developing novel hCT derived cell-penetrating peptides with improved metabolic stability. *Biochim Biophys Acta*. 2006;1758(3):347-354. doi:10.1016/j.bbamem.2005.10.006

12. Linde Y, Ovadia O, Safrai E, et al. Structure–activity relationship and metabolic stability studies of backbone cyclization and *N*-methylation of melanocortin peptides. *Biopolymers*. 2008;90(5):671-682. doi:10.1002/bip.21057

13. Chatterjee J, Gilon C, Hoffman A, Kessler H. *N*-Methylation of peptides: a new perspective in medicinal chemistry. *Acc Chem Res*. 2008; 41(10):1331-1342. doi:10.1021/ar8000603

14. Hewitt WM, Leung SSF, Pye CR, et al. Cell-permeable cyclic peptides from synthetic libraries inspired by natural products. *J Am Chem Soc*. 2015;137(2):715-721. doi:10.1021/ja508766b

15. Bockus AT, Schwochert JA, Pye CR, et al. Going out on a limb: delineating the effects of β-branching, *N*-methylation, and side chain size on the passive permeability, solubility, and flexibility of sanguinamide a analogues. *J Med Chem*. 2015;58(18):7409-7418. doi:10.1021/acs.jmedchem.5b00919

16. Patel SG, Sayers EJ, He L, et al. Cell-penetrating peptide sequence and modification dependent uptake and subcellular distribution of green florescent protein in different cell lines. *Sci Rep*. 2019;9(1):1-9. doi:10.1038/s41598-019-42456-8

17. Furukawa A, Schwochert J, Pye CR, et al. Drug-like properties in macrocycles above MW 1000: backbone rigidity versus side-chain lipophilicity. *Angew Chem Int Ed*. 2020;59(48):21571-21577. doi:10.1002/anie.202004550

18. Li Y, Li W, Xu Z. Improvement on permeability of cyclic peptide/peptidomimetic: backbone *N*-methylation as a useful tool. *Mar Drugs*. 2021;19(6):311. doi:10.3390/md19060311

19. Neer RHPV, Dranchak PK, Liu L, et al. Serum-stable and selective backbone-*N*-methylated cyclic peptides that inhibit prokaryotic

glycolytic mutases. *ACS Chem Biol*. 2022;17(8):2284-2295. doi:10.1021/acschembio.2c00403

20. Dougherty PG, Sahni A, Pei D. Understanding cell penetration of cyclic peptides. *Chem Rev*. 2019;119(17):10241-10287. doi:10.1021/acs.chemrev.9b00008

21. Francisco S, Chammaa S, Ruiz AS, Ortiz LM, Herrera FJL. Chemistry and biology of cyclic depsipeptides of medicinal and biological interest. *Curr Med Chem*. 2004;11(10):1309-1332. doi:10.2174/0929867043365224

22. Dang T, Süssmuth RD. Bioactive peptide natural products as lead structures for medicinal use. *Acc Chem Res*. 2017;50(7):1566-1576. doi:10.1021/acs.accounts.7b00159

23. Ribeiro R, Pinto E, Fernandes C, Sousa E. Marine cyclic peptides: antimicrobial activity and synthetic strategies. *Mar Drugs*. 2022;20(6):397. doi:10.3390/md20060397

24. Schwarze SR, Hruska KA, Dowdy SF. Protein transduction: unrestricted delivery into all cells? *Trends Cell Biol*. 2000;10(7):290-295. doi:10.1016/S0962-8924(00)01771-2

25. Fuchs SM, Raines RT. Internalization of cationic peptides: the road less (or more?) traveled. *Cell Mol Life Sci*. 2006;63(16):1819-1822. doi:10.1007/s00018-006-6170-z

26. Copolovici DM, Langel K, Eriste E, Langel Ü. Cell-penetrating peptides: design, synthesis, and applications. *ACS Nano*. 2014;8(3):1972-1994. doi:10.1021/nn4057269

27. Dupont E, Prochiantz A, Joliot A. Penetratin story: An overview. In: Langel Ü, ed. *Cell-Penetrating Peptides: Methods and Protocols*. New York, NY: Springer New York; 2015:29-37. doi:10.1007/978-1-4939-2806-4_2

28. Zhu P, Jin L. Cell penetrating peptides: a promising tool for the cellular uptake of macromolecular drugs. *Curr Protein Pept Sci*. 2018;19(2):211-220. doi:10.2174/1389203718666170710115240

29. Derakhshankhah H, Jafari S. Cell penetrating peptides: a concise review with emphasis on biomedical applications. *Biomed Pharmacother*. 2018;108:1090-1096. doi:10.1016/j.biopha.2018.09.097

30. Reineke TM, Raines RT, Rotello VM. Delivery of proteins and nucleic acids: achievements and challenges. *Bioconjug Chem*. 2019;30(2):261-262. doi:10.1021/acs.bioconjchem.9b00096

31. Xie J, Bi Y, Zhang H, et al. Cell-penetrating peptides in diagnosis and treatment of human diseases: from preclinical research to clinical application. *Front Pharmacol*. 2020;11:11. doi:10.3389/fphar.2020.00697

32. Zorko M, Langel Ü. Studies of cell-penetrating peptides by biophysical methods. *Q Rev Biophys*. 2022;55:e3. doi:10.1017/S0033583522000026

33. Wender PA, Mitchell DJ, Pattabiraman K, Pelkey ET, Steinman L, Rothbard JB. The design, synthesis, and evaluation of molecules that enable or enhance cellular uptake: Peptoid molecular transporters. *Proc Natl Acad Sci U S A*. 2000;97(24):13003-13008. doi:10.1073/pnas.97.24.13003

34. Tan NC, Yu P, Kwon Y-U, Kodadek T. High-throughput evaluation of relative cell permeability between peptoids and peptides. *Bioorg Med Chem*. 2008;16(11):5853-5861. doi:10.1016/j.bmc.2008.04.074

35. Calabretta LO, Thomas VM, Raines RT. Canavanine versus arginine: prospects for cell-penetrating peptides. *Tetrahedron Lett*. 2022;99:153848. doi:10.1016/j.tetlet.2022.153848

36. Mitchell DJ, Steinman L, Kim DT, Fathman CG, Rothbard JB. Polyarginine enters cells more efficiently than other polycationic homopolymers. *J Pept Res*. 2000;56(5):318-325. doi:10.1034/j.1399-3011.2000.00723.x

37. Rothbard JB, Jessop TC, Lewis RS, Murray BA, Wender PA. Role of membrane potential and hydrogen bonding in the mechanism of translocation of guanidinium-rich peptides into cells. *J Am Chem Soc*. 2004;126(31):9506-9507. doi:10.1021/ja0482536

38. Grogg M, Hilvert D, Beck AK, Seebach D. Syntheses of cyanophycin segments for investigations of cell-penetration. *Synthesis*. 2019;51(1):31-39. doi:10.1055/s-0037-1610202

39. White KN, Konopelski JP. Facile synthesis of highly functionalized *N*-methyl amino acid esters without side-chain protection. *Org Lett*. 2005;7(19):4111-4112. doi:10.1021/ol051441w

40. Carpino LA, Shroff H, Triolo SA, Mansour E-SME, Wenschuh H, Albericio F. The 2,2,4,6,7-pentamethyldihydrobenzofuran-5-sulfonyl group (Pbf) as arginine side chain protectant. *Tetrahedron Lett*. 1993;34(49):7829-7832. doi:10.1016/S0040-4039(00)61487-9

41. Jin E, Zhang B, Sun X, et al. Acid-active cell-penetrating peptides for in vivo tumor-targeted drug delivery. *J Am Chem Soc*. 2013;135(2):933-940. doi:10.1021/ja311180x

42. Komarov IV, Ishchenko AY, Hovtvianitsa A, et al. Fast amide bond cleavage assisted by a secondary amino and a carboxyl group—a model for yet unknown peptidases? *Molecules*. 2019;24(3):572. doi:10.3390/molecules24030572

43. Palm K, Stenberg P, Luthman K, Artursson P. Polar molecular surface properties predict the intestinal absorption of drugs in humans. *Pharm Res*. 1997;14(5):568-571. doi:10.1023/A:1012188625088

44. Di L, Artursson P, Avdeef A, et al. The critical role of passive permeability in designing successful drugs. *ChemMedChem*. 2020;15(20):1862-1874. doi:10.1002/cmdc.202000419

45. Chatterjee J, Rechenmacher F, Kessler H. *N*-Methylation of peptides and proteins: an important element for modulating biological functions. *Angew Chem Int Ed*. 2013;52(1):254-269. doi:10.1002/anie.201205674

46. Zhang S, Prabpai S, Kongsaeree P, Arvidsson PI. Poly-*N*-methylated α-peptides: synthesis and X-ray structure determination of β-strand forming foldamers. *Chem Commun*. 2006;5(5):497-499. doi:10.1039/B513277K

47. Nagel YA, Raschle PS, Wennemers H. Effect of preorganized charge-display on the cell-penetrating properties of cationic peptides. *Angew Chem Int Ed*. 2017;56(1):122-126. doi:10.1002/anie.201607649

48. Kalafatovic D, Giralt E. Cell-penetrating peptides: design strategies beyond primary structure and amphipathicity. *Molecules*. 2017;22(11):1929. doi:10.3390/molecules22111929

49. Khalil IA, Kogure K, Futaki S, Harashima H. Octaarginine-modified liposomes: enhanced cellular uptake and controlled intracellular trafficking. *Int J Pharm*. 2008;354(1-2):39-48. doi:10.1016/j.ijpharm.2007.12.003

50. Tünnemann G, Ter-Avetisyan G, Martin RM, Stöckl M, Herrmann A, Cardoso MC. Live-cell analysis of cell penetration ability and toxicity of oligo-arginines. *J Pept Sci*. 2008;2008(4):469-476. doi:10.1002/psc.968

51. Peraro L, Kritzer JA. Emerging methods and design principles for cell-penetrant peptides. *Angew Chem Int Ed*. 2018;57(37):11868-11881. doi:10.1002/anie.201801361

52. Daniels DS, Schepartz A. Intrinsically cell-permeable miniature proteins based on a minimal cationic PPII motif. *J Am Chem Soc*. 2007;129(47):14578-14579. doi:10.1021/ja0772445

SUPPORTING INFORMATION

Additional supporting information can be found online in the Supporting Information section at the end of this article.